Results in Physics 76 (2025) 108412

Contents lists available at ScienceDirect

Results in Physics

journal homepage: www.elsevier.com/locate/rinp

The Wang–Landau study of the frustrated J_1-J_2 Ising model on the honeycomb lattice: Phase diagrams and residual entropy

Mouhcine Azhari [a,b,c], Hoseung Jang [d], Unjong Yu [d,*]

[a] Laboratory of Condensed Matter and Interdisciplinary Sciences (LaMCSc), Physics Department, Faculty of Sciences, Mohammed V University, Rabat, Morocco
[b] Fakultät für Mathematik und Naturwissenschaften Bergische Universität Wuppertal, 42097 Wuppertal, Germany
[c] École Royale Navale, Casablanca 20052, Morocco
[d] Department of Physics and Photon Science, Gwangju Institute of Science and Technology, Gwangju 61005, South Korea

ARTICLE INFO

Keywords:
Monte Carlo method
Ising model
Geometric frustration
Phase transition
Finite-size scaling

ABSTRACT

We investigate the full phase diagram of the frustrated J_1-J_2 Ising model on the two-dimensional honeycomb lattice, incorporating both nearest-neighbor interaction J_1 and next-nearest-neighbor interaction J_2 using the Wang–Landau Monte Carlo method combined with finite-size scaling analysis. We map out the zero- and finite-temperature phase diagrams as a function of J_2/J_1. From the entropy profile, we identify four distinct ground-state structures — ferromagnetic, antiferromagnetic, dimer, and stripe states — and confirm that the residual entropy scales linearly with the lattice's linear dimension in the stripe and dimer ground states. Our results suggest that the transition from the paramagnetic phase into the dimer or stripe phase changes its nature from first-order to continuous while the transition into the ferromagnetic or antiferromagnetic phase is continuous and belongs to the two-dimensional Ising universality class.

Introduction

Onsager's exact solution [1] of the two-dimensional Ising model [2] on a square lattice significantly advanced the understanding of statistical physics and phase transitions. Building on this foundation, extending the model to include next-nearest-neighbor (NNN) interactions (J_2) alongside nearest-neighbor (NN) interactions (J_1) has proven challenging, sparking continued interest and debate over its intriguing properties [3–30].

Despite its simplicity, the J_1-J_2 model exhibits a rich landscape of phenomena due to frustration, which is defined as the impossibility of simultaneously satisfying all the interactions between the individual elements (spins or particles) because of the lattice's geometric constraints or competing interactions [31–33]. This frustration, tunable by the ratio $R \equiv J_2/J_1$, leads to various intriguing phenomena such as rough energy landscapes, strong metastability, and slow relaxation to equilibrium [26,34]. Key outcomes include extensive ground-state degeneracy [32,33], unusual phase transitions [33–36], and nonzero residual entropy at zero temperature [29,37]. Furthermore, these properties have significant implications for diverse fields, including unconventional superconductivity [22,38,39], quantum computing [40], and energy storage [41].

The J_1-J_2 Ising model has been studied extensively on various lattices, each providing distinct perspectives on the interplay between frustration and spin order [3–30]. The specific geometry of the lattice further highlights the role of frustration and competing interactions in shaping the phase diagram. Experimentally, van der Waals magnets serve as essential systems for testing the J_1-J_2 Ising model on the honeycomb lattice. VBr_3 single crystals exhibit strong uniaxial anisotropy, a first-order spin-flip transition, and a tricritical point in magnetic fields [42]. Under pulsed fields up to 65 T, $FePS_3$ undergoes two successive first-order transitions, indicating significant exchange anisotropy [43]. Its Néel temperature remains almost unchanged at 118 K, even in the monolayer regime, as demonstrated by Raman spectroscopy [44]. Extensions of the model to include third-nearest-neighbor interactions J_3 predict frustration phenomena (residual entropy) and broad specific-heat maxima that correspond closely with experimental findings [45]. It is important to note that the simpler J_1-J_2 model already explains the zigzag-to-paramagnetic first-order transition observed in $FePS_3$ [46]. These findings link statistical mechanics to the specific behavior of materials, highlighting the ongoing relevance of the J_1-J_2 Ising model.

On the square lattice, the J_1-J_2 Ising model exhibits no frustration when NNN interactions are ferromagnetic (FM); the ground state is FM if NN interactions are FM, and antiferromagnetic (AFM) if they are AFM. For strong AFM NNN interactions $|R| > 1/2$, the ground state exhibits a stripe order (also called a super-antiferromagnetic order or a

* Corresponding author.
E-mail addresses: azhari.mouhcine@gmail.com (M. Azhari), uyu@gist.ac.kr (U. Yu).

https://doi.org/10.1016/j.rinp.2025.108412
Received 17 July 2025; Received in revised form 14 August 2025; Accepted 26 August 2025
Available online 1 September 2025

collinear order) [5,17,18]. However, the precise location of the critical line remains unknown [27]. At the special point $|R| = 1/2$, where the ground state changes from a FM or AFM state to a stripe state, it was proposed that the ground state degeneracy leads to disorder at all finite temperatures, resembling an Ising chain in a transverse field [10–12]. The nature of phase transitions near $|R| = 1/2$ is still controversial, despite several past studies (see recent studies [27,28] and references therein). Current evidences point to weakly first-order transitions for $|R| \gtrsim 0.67$ that become second-order asymptotically as $R \to +\infty$. For $0.5 \leq |R| \lesssim 0.67$, however, the nature of the transitions is still debated: some studies report a weak first-order character, while others find entirely second-order behavior.

On the other hand, the AFM Ising model on the triangular lattice is inherently frustrated even at $J_2 = 0$, leading to a spin-liquid ground state. Introducing NNN interactions relieves frustration and stabilizes exotic orders such as the $\sqrt{3}\times\sqrt{3}$ ferrimagnetic and collinear super-antiferromagnetic phases [3,6]. Notably, the phase transition from the paramagnetic phase into the collinear super-antiferromagnetic phase was reported to be first-order [13,14]. A recent work also shows that anisotropic or non-regular NNN interactions can induce intriguing properties such as ordering in reduced dimensions, partial-spin-liquid ground state, and successive phase transitions [29]. Exploring other lattice geometries may eventually provide a deep understanding of the nature of the ground states and phase transitions in the J_1-J_2 Ising model.

Compared to the square and triangular lattices, the honeycomb lattice has received much less attention in the context of the J_1-J_2 Ising model [19,23–25,30]. The honeycomb lattice offers a unique framework due to its bipartite, non-Bravais structure and a lower coordination number ($z = 3$), compared with those of the square ($z = 4$) and triangular ($z = 6$) lattices, which intensifies the frustration effect [47–49]. This supposition is further supported by exotic phases such as the spiral phase, a gapped spin liquid phase, and a lattice nematic phase, as reported in theoretical and experimental studies of the J_1-J_2 Heisenberg model on the honeycomb lattice [50–53]. While the J_1-J_2 Ising model on the honeycomb lattice has been explored through various methods like effective-field theory [19], Monte Carlo simulations (Metropolis and parallel tempering algorithms) [20,23], machine learning [24], cluster mean-field approach [25], and partition function zeros [30], the phase diagram remains incomplete, highlighting the challenges of studying highly frustrated systems. It is noteworthy that the tricritical point predicted around $R = -0.1$ by effective-field theory [19] has not been confirmed in subsequent studies [23,25,30].

In this paper, we construct the full phase diagram of the J_1-J_2 Ising model on the honeycomb lattice using the Wang–Landau (WL) algorithm [54], a novel approach for this system. Our study focuses on elucidating the effects of competing interactions J_1 and J_2 on the system. Specifically, we present an entropy profile and residual entropies to identify ground states and investigate the nature of phase transitions and critical phenomena in the model.

This paper is organized as follows. In Section ‘Model and methods’, we provide a concise overview of the model and the methods employed in this study. Section ‘Results and Discussion’ presents and discusses our numerical results, including the phase diagram and critical properties. Finally, Section ‘Conclusion’ summarizes our findings and offers concluding remarks.

Model and methods

The J_1-J_2 Ising model with competing NN and NNN interactions is described by the Hamiltonian

$$H = -J_1 \sum_{\langle i,j\rangle} s_i s_j - J_2 \sum_{\langle\langle i,j\rangle\rangle} s_i s_j, \tag{1}$$

where $\langle\cdot\rangle$ and $\langle\langle\cdot\rangle\rangle$ respectively denote NN and NNN spin pairs, and $s_i = \pm 1$ is the Ising spin variable at the ith site of a two-dimensional honeycomb lattice. Positive (*resp.* negative) values of exchange couplings J_1 and J_2 correspond to FM (*resp.* AFM) interactions. To reduce surface effects, we consider a honeycomb lattice of $N = L^2$ spins with periodic boundary conditions in both directions, where L is the linear size of the lattice. Only even values of L are considered to ensure the correct application of periodic boundary conditions along both directions. Although the honeycomb lattice is typically defined with a two-site basis ($N = 2L^2$) [48], we adopted an effective four-site basis in this work. This choice helps us to construct lattices with squareness close to 1 easily, thereby reducing potential finite-size effects [55,56].

Since no exact solution exists for the model in Eq. (1) for a nonzero J_2, we employed the Monte Carlo method to compute the observables. Specifically, we calculated the ensemble average of absolute magnetization m, magnetic susceptibility χ, specific heat C, and Binder cumulant U [57] as functions of temperature T, which are defined as

$$m = \frac{1}{N}\left\langle \left| \sum_{i=1}^{N} s_i \right| \right\rangle, \tag{2}$$

$$\chi = \frac{N}{k_B T}\left(\left\langle m^2 \right\rangle - \langle m\rangle^2 \right), \tag{3}$$

$$C = \frac{N}{(k_B T)^2}\left(\left\langle E^2 \right\rangle - \langle E\rangle^2 \right), \tag{4}$$

$$U = 1 - \frac{\left\langle m^4 \right\rangle}{3\left\langle m^2 \right\rangle^2}, \tag{5}$$

where $E = H/N$ denotes the energy per spin and $\langle\cdots\rangle$ means the ensemble average. Throughout this paper, we set the Boltzmann constant k_B to unity ($k_B = 1$) without loss of generality, so that temperature is expressed in energy units.

The Metropolis algorithm [58] is widely used to simulate systems in the Boltzmann distribution due to its simplicity and broad applicability. However, the algorithm often struggles to efficiently explore the complex energy landscape near first-order phase transitions or in highly frustrated systems due to supercritical slowing-down [59], leading to difficulties in accurately capturing the emergence of phase transitions. The Metropolis algorithm performs poorly in the highly frustrated regime $J_2 < 0$ and $|R| \gtrsim 0.20$ of the current model, revealing extremely slow dynamics and bad convergence to equilibrium as reported recently in Ref. [23]. To resolve these challenges, we applied the WL algorithm [54], which can overcome high energy barriers and improve convergence to equilibrium. The WL algorithm has been adopted in several recent studies in statistical mechanics, where it has been proven to be efficient and reliable in determining the entropy profile and phase diagrams in frustrated systems and complex social dynamics [18,60–64].

Thus, we used the WL algorithm to determine the entropy profile, ground states, and the phase diagram of the J_1-J_2 Ising model on the honeycomb lattice. For more comprehensive discussions of the method, a detailed explanation of the approach is provided in Refs. [60,61]. The WL method requires knowledge of the density of states (DOS) $\rho(E_1, E_2)$, which is estimated numerically through a random walk in the energy space (E_1, E_2), where $E_1 = (\sum_{\langle i,j\rangle} s_i s_j)/N$ and $E_2 = (\sum_{\langle\langle i,j\rangle\rangle} s_i s_j)/N$; the total energy per spin is given by $E = -J_1 E_1 - J_2 E_2$. The reciprocal of the DOS is used as the sampling probability function: the transition probability is defined by

$$P(I \to F) = \min\left[1, \frac{\rho\left(E_1^{(I)}, E_2^{(I)}\right)}{\rho\left(E_1^{(F)}, E_2^{(F)}\right)}\right], \tag{6}$$

where $\left(E_1^{(I)}, E_2^{(I)}\right)$ and $\left(E_1^{(F)}, E_2^{(F)}\right)$ are energy components before and after the transition. At each Monte Carlo step, the DOS $\rho(E_1, E_2)$ is multiplied by the empirical modification factor λ_n ($\lambda_n > 1$) while simultaneously updating the histogram $h(E_1, E_2)$. The histogram gradually flattens as the simulation progresses. Once the standard deviation of $h(E_1, E_2)$ for all accessible combinations of (E_1, E_2) is less than 4% of the average histogram value, a new set of random walks begins with an empty histogram and a reduced modification factor following the rule $\lambda_{n+1} = \sqrt{\lambda_n}$. Starting with $\lambda_0 = e$, the simulation continues until the final modification factor $\lambda_n < \exp(10^{-10})$, at which point the final DOS $\rho(E_1, E_2)$ reaches an accurate version quite close to the true DOS. After normalizing such that $\sum_{E_1,E_2} \rho(E_1, E_2) = 2^N$, we obtain the entropy of each state as $S(E_1, E_2) = \log[\rho(E_1, E_2)]$ [48,49]. The residual entropy (or zero-point entropy) $S_0 = S(E_1^{(g)}, E_2^{(g)})$ represents the entropy at zero temperature, where $E_1^{(g)}$ and $E_2^{(g)}$ are the values of E_1 and E_2 of the ground state. After determining $\rho(E_1, E_2)$, we compute the average observable $O(E_1, E_2)$ through additional WL iterations. Finally, ensemble averages $\langle O(T, J_1, J_2)\rangle$ of any thermodynamic variable can be computed for arbitrary temperature (T) and coupling constants (J_1 and J_2) using the determined $\rho(E_1, E_2)$ and $O(E_1, E_2)$ by

$$\langle O(T, J_1, J_2)\rangle = \frac{\sum_{E_1,E_2} O(E_1, E_2)\rho(E_1, E_2)\, e^{\frac{(J_1E_1+J_2E_2)N}{T}}}{\mathcal{Z}(T, J_1, J_2)} \tag{7}$$

with the partition function

$$\mathcal{Z}(T, J_1, J_2) = \sum_{E_1,E_2} \rho(E_1, E_2)\, e^{\frac{(J_1E_1+J_2E_2)N}{T}}. \tag{8}$$

For each system size L, we performed five independent runs and averaged both $\rho(E_1, E_2)$ and $O(E_1, E_2)$. Since the WL algorithm does not suffer from the critical and supercritical slowing-down, it ensures reliable results even in frustrated systems, making it particularly efficient for constructing phase diagrams in such systems [60,61].

Because the energy space scales as L^4, computational constraints limit the maximum lattice size to $L = 24$. Calculating $\rho(E)$ with $E = -J_1E_1 - J_2E_2$ instead of $\rho(E_1, E_2)$ may reduce the size of the energy space, thereby allowing calculations in larger lattices, especially when J_1 and J_2 have a simple integer ratio. In particular, at $R = -0.5$, the two-dimensional energy space (E_1, E_2) collapses to a single dimension ($E = -J_1(E_1 - E_2/2)$), enabling calculation in lattices up to $L = 48$.

For larger lattice sizes, we utilized the Metropolis algorithm [58]. Due to its limitations in highly frustrated systems, we restricted its use to weakly frustrated cases where we could validate results against those of WL simulations. Each simulation involved 2×10^7 Monte Carlo steps per temperature, preceded by 2×10^6 equilibration steps, with one spin-flip attempt per spin per Monte Carlo step. In order to minimize thermalization time, temperatures were varied slowly, and each new run was initialized with the final spin configuration from the previous temperature. To ensure consistency, we performed simulations with both increasing and decreasing temperature sweeps; any results exhibiting hysteresis were discarded. Near critical temperatures, we increased the number of iterations by up to fivefold to compensate for the effects of critical slowing down. Within the Metropolis algorithm, the residual entropy can also be calculated through the measurement of the specific heat [65,66] by doing a numerical integration as

$$S_0 = N\left[\log(2) - \int_0^\infty \frac{C(T)}{T}\,dT\right]. \tag{9}$$

This method becomes numerically unstable for large N, as the phase transition peak grows sharper with increasing system size, while the Metropolis algorithm only provides data at discrete temperatures. Due to these limitations, our analysis is restricted to small lattices ($L \le 48$). It is worth noting that the instability in Eq. (9) can be circumvented by employing an alternative energy-integration-based formula [67].

To determine the critical temperature T_c, we employed two complementary approaches. The first method identifies T_c from the crossing point of Binder cumulants U for different system sizes [61,62,68,69], which applies to both continuous and first-order transitions. However, this method can be applied only to systems in which magnetization serves as a valid order parameter or where an appropriate order parameter has been defined. The second approach determines T_c through finite-size scaling (FSS) fitting of the pseudo-critical temperature $T_c(L)$, which is defined as the peak position of the susceptibility or the specific heat, to

$$\left[T_c(L) - T_c\right] \propto L^{-1/\nu}. \tag{10}$$

In the latter method, the correlation length exponent ν is determined simultaneously. We confirmed that the two methods yield equivalent results within error bars. Additionally, critical exponents ν and γ/ν can be determined from the maxima of $|dU/dT|$ and χ of various lattice sizes [70]:

$$\text{Max}\left[\left|\frac{dU}{dT}\right|\right] \propto L^{1/\nu} \tag{11}$$

$$\text{Max}\left[\chi\right] \propto L^{\gamma/\nu}. \tag{12}$$

The derivative of the Binder cumulant can be calculated by

$$\frac{dU}{dT} = \frac{2\langle m^4\rangle\langle Hm^2\rangle - \langle H\rangle\langle m^4\rangle\langle m^2\rangle - \langle Hm^4\rangle\langle m^2\rangle}{3T^2\langle m^2\rangle^3}. \tag{13}$$

Results and discussion

In Fig. 1(b), we present the zero-temperature global phase diagram of the Ising model with NN coupling J_1 and NNN coupling J_2 on the honeycomb lattice, obtained from the entropy profile in Fig. 1(a). The entropy $S(E_1, E_2)$ is symmetric about $E_1 = 0$, which is expected given the bipartite nature of the honeycomb lattice. This mirror symmetry in the entropy profile is also reflected in the phase diagram in Fig. 1(b), which is symmetric about $J_1 = 0$. At zero temperature, the dominant contribution comes from the minimum of the total energy per site $E = -J_1E_1 - J_2E_2$, as outlined in Eq. (7). Therefore, the values of E_1 and E_2 of the ground state for given J_1 and J_2 are determined straightforwardly. In the entropy profile, the four corner points — ($E_1 = 1.5, E_2 = 3$), ($E_1 = -1.5, E_2 = 3$), ($E_1 = -0.5, E_2 = -1$), and ($E_1 = 0.5, E_2 = -1$) — correspond to the FM, AFM, dimer, and stripe ground states, respectively. The phase boundaries manifest themselves geometrically as the slopes of the outer edges in the entropy profile. The phase boundaries in Fig. 1(b) represent the energy crossover $E_{\text{FM}} = E_{\text{ST}}$ (*resp.* $E_{\text{AFM}} = E_{\text{D}}$) at $J_2 = -0.25J_1$ (*resp.* $J_2 = 0.25J_1$). Along each boundary, all states on the straight line connecting the corresponding vertices share the same energy per site ($E = -0.75|J_1|$), signaling an extensive ground-state degeneracy.

The FM and AFM ground states exhibit conventional twofold degeneracy due to global spin inversion symmetry. Thus, the residual entropy per spin is

$$S_0/N = \lim_{N\to\infty} (\log 2)/N = 0 \tag{14}$$

in the thermodynamic limit. By contrast, the dimer and stripe ground states, which are the result of strong frustration, exhibit much greater degeneracy. This leads to a residual entropy that grows linearly with the system size L. In the stripe phase, any spin configuration satisfying $E_1 = 0.5$ and $E_2 = -1$ could be the ground state. In other words, the ground state must satisfy a simple local rule: every spin must have exactly two parallel and one antiparallel NN spins, and two parallel and four antiparallel NNN spins. This local rule provides a straightforward criterion for identifying the stripe ground state configurations located in the fourth quadrant of Fig. 1(b). These horizontal stripe states consist of alternating up and down spin stripes, which can bend along either rising or falling diagonals. The bending of a single stripe leads to 2^L distinct configurations for a system of size L. Once the path of one stripe is fixed, the configurations of the remaining stripes are fully determined by the imposed constraints. Therefore, the residual entropy of the horizontal stripe state is $S_0 = \log[2^L] = (\log 2)L$. Vertical stripe states, which consist of alternating up and down spins in straight vertical stripes, also obey the same ground-state spin rule. However, because they cannot bend, their degeneracy is limited to two, and their contribution to the total residual entropy is negligible. This finding is supported by the plot in Fig. 1(c), where the residual

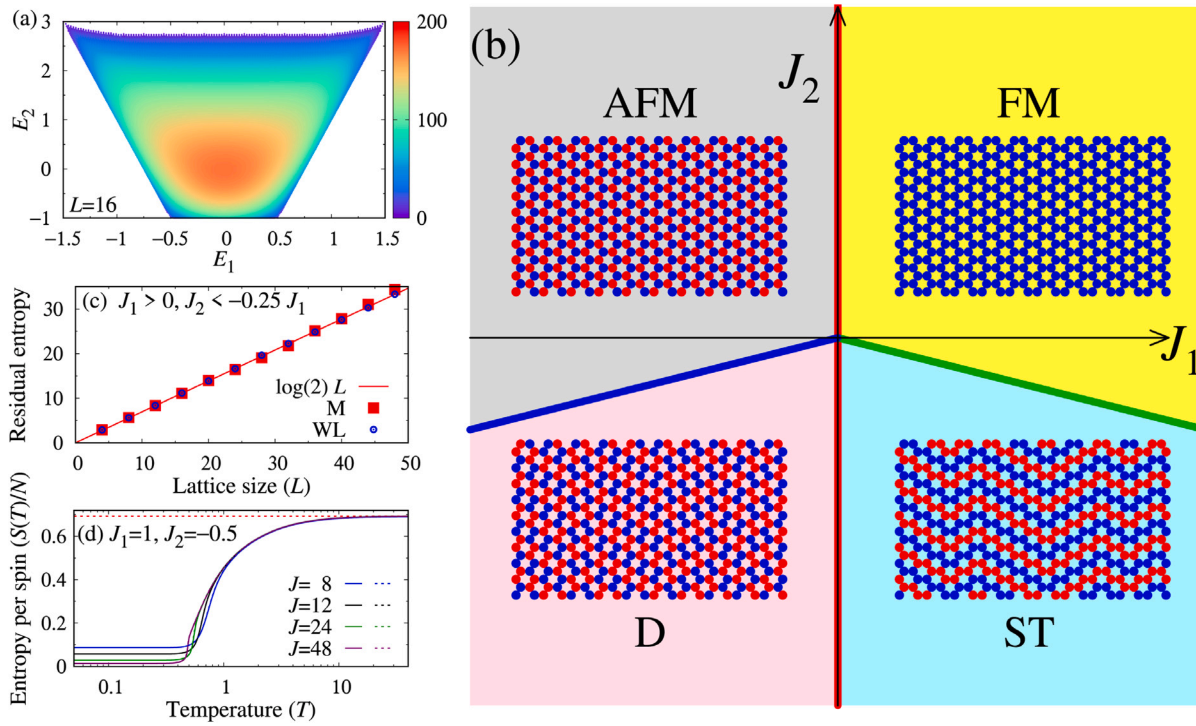

Fig. 1. (a) Entropy profile as a function of E_1 and E_2 for the J_1-J_2 Ising model in the honeycomb lattice of $L = 16$. (b) Zero-temperature phase diagram as a function of J_1 and J_2. Yellow, gray, pink, and light cyan colors represent regions where the ground state is ferromagnetic (FM), antiferromagnetic (AFM), dimer (D), and stripe (ST) phases, respectively. The green and blue lines indicate the phase boundaries of $J_2 = -0.25|J_1|$. Typical spin configurations for each ground state are presented, where blue and red circles represent up and down spins, respectively. (c) Residual entropy (S_0) of the stripe ground state observed for $J_1 > 0$ and $J_2 < -0.25J_1$. Filled squares were calculated by the Metropolis (M) algorithm at $J_1 = 1$ and $J_2 = -0.5$ through Eq. (9), and open circles were obtained from the Wang–Landau (WL) algorithm. The statistical errors are comparable to the size of the symbols. The red straight line represents $S_0 = [\log(2)]L$. (d) Entropy per spin as functions of temperature for $J_1 = 1$ and $J_2 = -0.5$. Results obtained using the Metropolis method (dotted lines) and the WL method (solid lines) are visually indistinguishable. The red horizontal line denotes the high temperature limit $\lim_{T\to\infty} S(T)/N = \log(2)$.

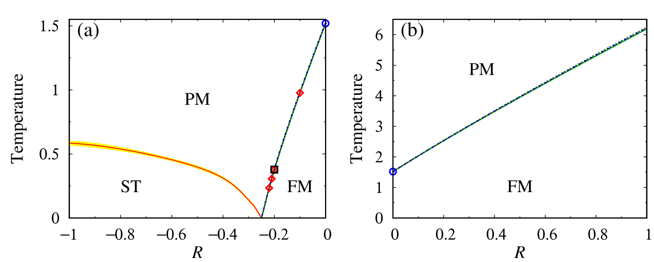

Fig. 2. Finite-temperature phase diagram for $J_1 = 1$ and $R = J_2/J_1$. PM, ST, and FM represent paramagnetic, stripe, and ferromagnetic states, respectively. The phase diagram for $J_1 = -1$ and $R = J_2/|J_1|$ is obtained by replacing FM with AFM (antiferromagnetic state) and ST with D (dimer state). The exact value [71,72] of $T_c = 2/\log(2+\sqrt{3})$ at $R = 0$ is represented as the empty circle. The empty square and empty diamonds denote the values of T_c obtained by the parallel tempering with finite-size scaling in Ref. [23] and partition function zeros in Ref. [30]. For $R < -0.25$, T_c was calculated by the location of the maximum specific heat through Eq. (10). For $R > -0.25$, the green solid line denotes T_c obtained from the Binder cumulant crossing, the blue dotted line from the maximum susceptibility, and the black dashed line from the maximum specific heat. The yellow shaded region for $R < -0.25$ represents the standard error of T_c. For $R > -0.25$, the error bar is comparable to the line thickness.

entropy $S_0(L)$ aligns with $(\log 2)L$, which shows that the dominant part of the residual entropy is attributed to horizontal stripe states. Remarkably, the residual entropy data obtained by the WL algorithm and the Metropolis algorithm through Eq. (9) agree excellently. Fig. 1(d) shows entropy per spin $S(T)/N$ versus temperature T for $J_1 = 1$ and $J_2 = -0.5$. It approaches $\log(2)$ at high T and remains above zero at $T = 0$ due to nonzero residual entropy.

The same residual entropy appears in the dimer ground state, which emerges for $J_1 < 0$ and $J_2 < 0.25J_1$. Because the honeycomb lattice is bipartite, inverting all spins on one of the two bipartite sublattices is equivalent to reversing the sign of J_1. Hence, the transition temperature and residual entropy of the AFM and dimer states coincide with those of the FM and stripe states, respectively. Consequently, the residual entropy of the dimer state is approximately $S_0 = (\log 2)L$.

Fig. 2 shows the finite-temperature phase diagram as a function of $R = J_2/J_1$, with J_1 set to unity. With positive J_2 (the first and second quadrants in Fig. 1(b)), the NN and NNN interactions cooperate to stabilize FM or AFM ground states depending on the sign of J_1. As J_2 increases with $J_1 = 1$, T_c increases monotonically as shown in Fig. 2(b), and the phase transitions were confirmed to be continuous within the two-dimensional Ising universality class. Therefore, we focus on the fourth quadrant of Fig. 1(b) ($J_1 > 0$ and $J_2 < 0$), where the system is frustrated. By symmetry, the behavior in the third quadrant ($J_1 < 0$ and $J_2 < 0$) can be inferred from these results.

We first investigated the thermodynamic behavior for $-0.25 < R \le 0$ to examine signatures of phase transitions. Fig. 3 shows the temperature dependence of the absolute magnetization (m), magnetic susceptibility (χ), Binder cumulant (U), energy per spin (E), and specific heat (C) for $R = 0$, -0.2, and -0.24. All results exhibit features of continuous phase transitions. As R approaches the critical value $R = -0.25$, the effect of frustration becomes more pronounced and the phase transitions become sharper. However, we could not find any evidence of

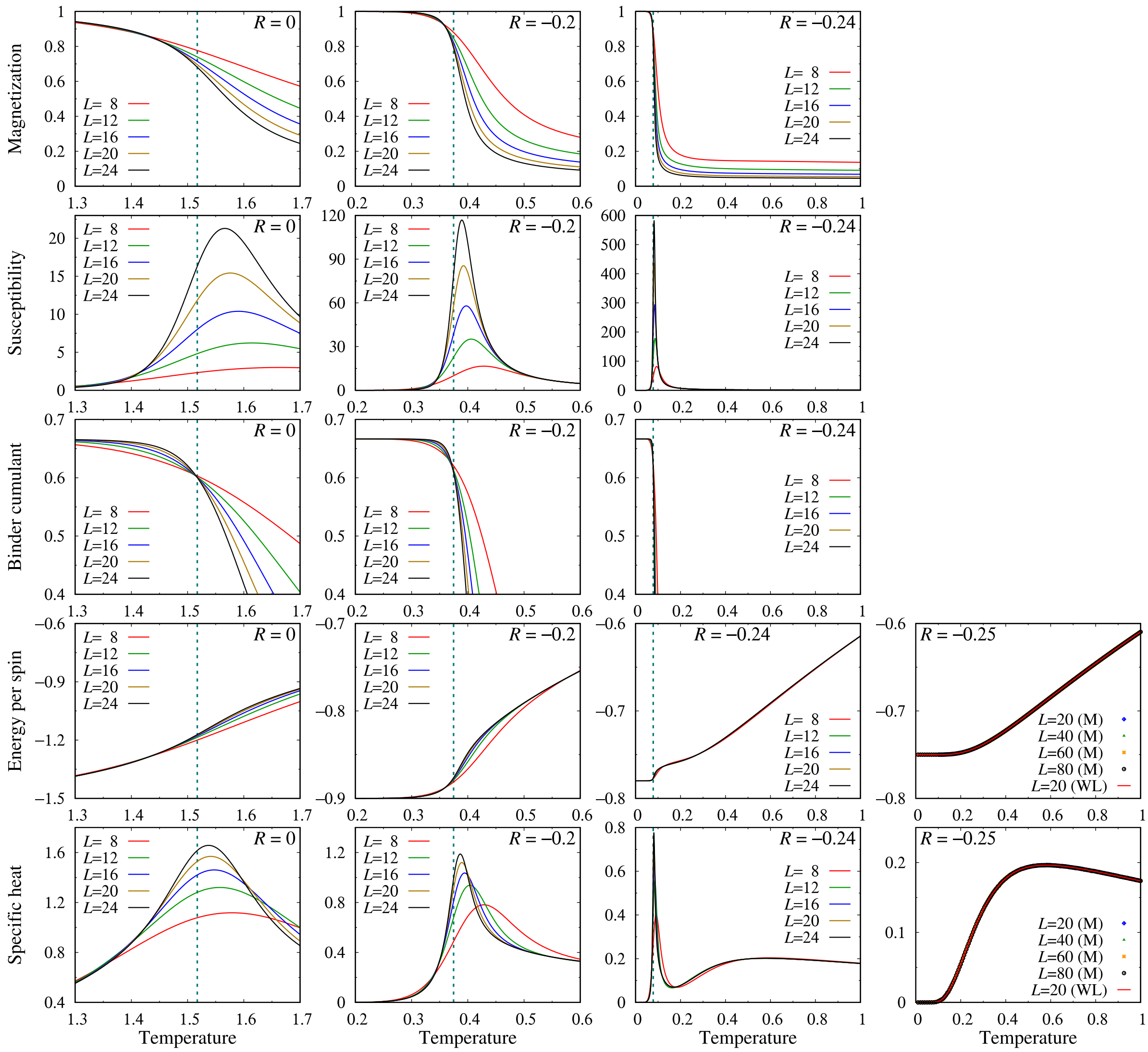

Fig. 3. Absolute magnetization (m), magnetic susceptibility (χ), Binder cumulant (U), energy per spin (E), and specific heat (C) as functions of temperature (T) for $J_1 = 1$ and $R = J_2/J_1$ varying the lattice size L. The vertical dotted lines represent the values of the critical temperatures of the infinite lattice obtained by the crossing of the Binder cumulant data for lattices of $L = 20$ and $L = 24$. All the results were calculated by the Wang–Landau (WL) algorithm except the symbols in the rightmost column, which were obtained by the Metropolis (M) algorithm. The statistical error is smaller than the symbol size or the line width.

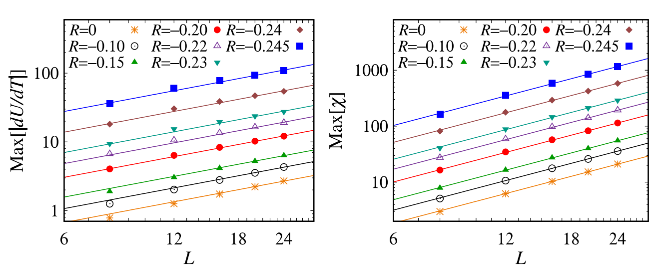

Fig. 4. The maximum values of $|dU/dT|$ and susceptibility χ as functions of the lattice size L for various values of R in the range $-0.25 < R \leq 0$, with $J_1 = 1$. Since both x- and y-axes are in logarithmic scales, the slopes of the straight lines are $1/\nu = 1$ in the left panel and $\gamma/\nu = 1.75$ in the right panel. The statistical error is smaller than the symbol size.

a first-order phase transition in the energy histogram and the Binder cumulant. It is worth mentioning that a previous Monte Carlo study reported that reliable determination of the transition type and the transition temperatures in the range $-0.25 < R \lesssim -0.2$ was hindered by extremely slow dynamics and bad convergence to equilibrium in this region [23]. We calculated the critical exponents ν and γ/ν within the range $-0.245 \leq R \leq 0$ using the scaling relation in Eqs. (11)–(12). As shown in Fig. 4, the extracted values of critical exponents ν and γ/ν align well with those of the unfrustrated two-dimensional Ising universality class ($\nu = 1$ and $\gamma/\nu = 1.75$ [1]). This agreement is particularly clear for large lattices ($L \geq 16$), where finite-size effects are reduced. Note that these results are consistent with the results of a recent study of partition function zeros for $R = -0.1$, -0.2, -0.21 and -0.22 [30]. Therefore, it would be reasonable to conclude that the phase transitions for $R > -0.25$ are continuous within the Ising universality class, and that no tricritical point exists in this regime.

We determined the critical temperature T_c in the thermodynamic limit ($L \to \infty$) by locating the crossing point of the Binder cumulant U between the two largest lattices used in this work ($L = 20$ and $L = 24$) for $R > -0.25$. These values of T_c agree within 1% with those obtained by fitting the peak positions of C and χ to Eq. (10). In Fig. 2, the green solid, blue dotted, and black dashed lines represent T_c values obtained from the Binder cumulant crossing point, the maximum of the susceptibility, and the maximum of the specific heat, respectively. At $R = 0$, the critical point is exactly known from analytical results [71,72],

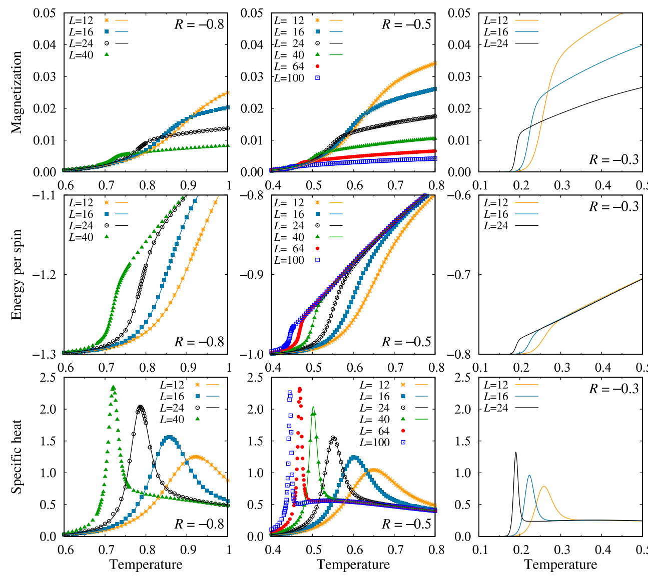

Fig. 5. Absolute magnetization (m), energy per spin (E), and specific heat (C) as functions of temperature (T) for $J_1 = 1$ and $R = J_2/J_1 = \{-0.8, -0.5, -0.3\}$ varying the lattice size L. Symbols and lines represent results obtained by the Metropolis (M) and Wang–Landau (WL) algorithms, respectively. The results of the Metropolis algorithm are omitted for $R = -0.3$, where strong hysteresis occurs. The statistical error is smaller than the symbol size or the line width.

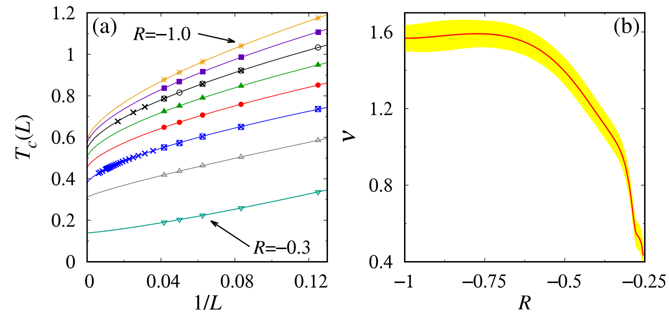

Fig. 6. (a) Temperatures that maximize the specific heat as a function of inverse lattice size ($1/L$) for given $R = J_2/J_1$ with $J_1 = 1$. The data series correspond to $R = -1.0$, -0.9, -0.8, -0.7, -0.6, -0.5, -0.4, and -0.3 from top to bottom. Symbols denote results via the Wang–Landau algorithm, except for crosses ($\times$), which represent results via the Metropolis algorithm. Solid lines are fits to Eq. (10). (b) The values of ν obtained by the fitting as a function of R. The yellow shading behind the solid line represents the standard error of ν.

corresponding to a transition from the paramagnetic phase into the FM phase at $T_c = 2/\log(2+\sqrt{3})$. For $R \in \{-0.22, -0.21, -0.20, -0.10\}$, our T_c estimates are consistent with previous works, which used the parallel tempering method [23] and the partition function zeros method [30]. The effective-field theory [19] and the cluster mean-field approximation [25] also yield qualitatively similar phase diagrams for $-0.25 \le R$ but tend to significantly overestimate the critical temperature ($T_c \approx 1.87$ and $T_c \approx 2.20$, respectively, at $R = 0$). As R decreases, T_c decreases and vanishes at $R = -0.25$.

In the rightmost column of Fig. 3, we display the temperature dependence of the energy and the specific heat at the critical point ($R = -0.25$), where the two ordered phases (FM and stripe), along with all states lying on the straight line connecting them in Fig. 1(a), are degenerate at zero temperature. It demonstrates a distinct behavior from that observed in the square lattice at its critical point $R = \pm 0.5$ [15,18,21]. For the honeycomb lattice, no size-dependent peaks of C are observed at $R = -0.25$, indicating the absence of long-range order and of a finite-temperature phase transition, owing to the extremely high ground-state degeneracy with extensive residual entropy ($S_0 \propto N$). The size-independent broad peak in specific heat around $T = 0.5$ persists in highly frustrated region centered at $R = -0.25$, producing a two-peak structure in the ranges $-0.31 \le R < -0.25$ and $-0.25 < R \le -0.23$ for $L = 24$. The size-dependent sharp peak at lower temperatures arises from a phase transition, whereas the size-independent broad peak at higher temperatures originates from short-range correlations associated with frustration effects [25].

For $R < -0.25$, the system undergoes a finite-temperature transition into a stripe-ordered state, with T_c rising as R becomes more negative. For $J_1 = 0$ and $J_2 < 0$, the system reduces to the triangular-lattice antiferromagnet, which exhibits no finite-temperature phase transition [71]. Thus, in the limit $R \to -\infty$ with $J_1 = 1$, $T_c/|J_2|$ is expected to approach zero. Since no proper order parameter is defined, the transition temperatures were determined solely by extrapolating the specific-heat peak position to $L \to \infty$ via Eq. (10). Consequently, the uncertainty in T_c, which is represented by the yellow shaded region in Fig. 2(a), is relatively large. Fig. 5 shows the temperature dependence of the absolute magnetization (m), energy per spin (E), and specific heat (C) for $R = -0.8$, -0.5, and -0.3. The sharpening of the specific-heat peak with increasing lattice size signals the onset of stripe ordering. For weakly frustrated cases $R \le -0.5$, the Metropolis algorithm was also used to overcome the computational constraints of the WL method. In Fig. 5, symbols and lines denote results obtained by the Metropolis and WL algorithms, respectively; the two approaches yield consistent results within statistical error. In the strongly frustrated case ($R = -0.3$), the Metropolis algorithm fails to reach the ground state, becoming trapped in metastable states separated by high energy barriers.

Fig. 6 presents fits of the finite-size specific-heat peak positions $T_c(L)$. Extrapolating $T_c(L)$ to $1/L \to 0$ yields both the critical temperature in the thermodynamic limit and the correlation-length exponent ν. As shown in Fig. 6(b), for $R < -0.25$, the exponent ν deviates from that of the two-dimensional Ising model ($\nu = 1$) and varies continuously with R. The data of large lattices for $R = -0.5$ and $R = -0.8$ in Fig. 6(a) unequivocally indicate the discrepancy from the linear behavior expected for $\nu = 1$. Therefore, it is clear that the phase transitions into the stripe state for $R < -0.25$ do not belong to the Ising universality class. Notably, similar deviations from the Ising universality class have been reported in other frustrated systems, such as the stripe transitions in the square-lattice Ising model [16,17] and the AFM Ising model on the trellis lattice [48]. The mechanism behind this behavior and its connection to the Ashkin–Teller model [73,74] or to Ashkin–Teller criticality observed in the square-lattice J_1-J_2 Ising model [16,17] are beyond the scope of the present work.

In Fig. 7, we present the energy histograms near the pseudo-critical temperature $T_c(L)$, obtained by the WL algorithm for $L = 24$ at three representative values of $R \in \{-0.5, -0.4, -0.3\}$. For $R = -0.3$, the histogram exhibits a clear two-peak structure. As the temperature decreases, the lower-energy peak gains weight while the higher-energy peak diminishes, which indicates a first-order phase transition [62,75]. It is worth noting that the double-peak structure, which is clear in small lattices, sometimes disappears in large lattices [61,76]. However, the probability density is practically zero in the gap between the two peaks and the gap width is large enough, we conjecture the double-peak structure will pertain also in the thermodynamic limit. In contrast, the histogram for $R = -0.5$ shows a single peak structure, where the peak moves continuously with temperature, characteristic of a continuous phase transition. For an intermediate case $R = -0.4$, the histogram displays hybrid features of first-order and continuous transitions, pointing to a tricritical point nearby. Determining its precise location is beyond the scope of this work, but our data strongly indicate that it lies between $R = -0.5$ and $R = -0.3$. In contrast, for $R > -0.25$ the transitions remain continuous and fall within the two-dimensional Ising universality class.

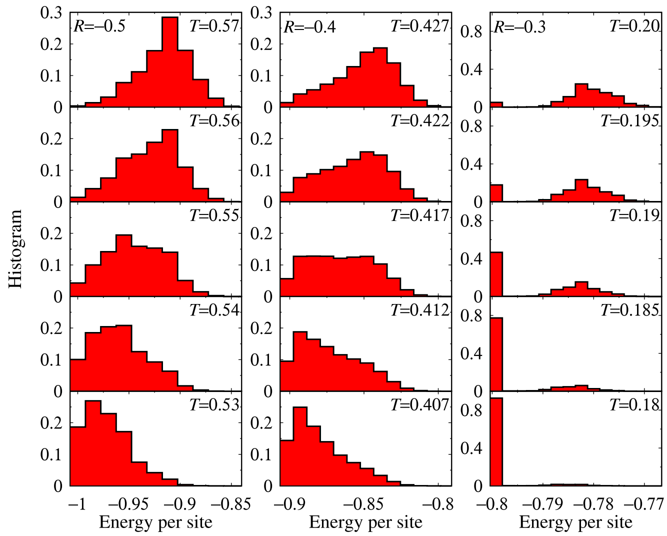

Fig. 7. Histogram as a function of energy near the pseudo critical temperature $T_c(L)$ with $L = 24$ for $J_1 = 1$ and $R = \{-0.5, -0.4, -0.3\}$ from left to right, obtained via the Wang–Landau algorithm. The histogram is normalized such that the sum of all bin values equals unity.

Conclusion

We studied the frustrated J_1-J_2 Ising model in the two-dimensional honeycomb lattice using Monte Carlo methods. The WL algorithm provided the entropy profile and phase diagrams across the full range of frustration ratios $R \equiv J_2/J_1$, while the Metropolis algorithm allowed us to explore larger lattices in the weakly frustrated regime. Stripe and dimer ground states are stabilized in $J_2 < 0$ and $|R| > 0.25$, and FM and AFM ground states were found in the other regime. The residual entropy of the stripe and dimer ground states scales linearly with the lattice's linear dimension L. This can be explained by the bending of the stripe and dimer patterns in the ground states.

We also constructed the finite-temperature phase diagram by calculating the critical temperature for ordering into each ground state. Transitions into the FM and AFM phases are continuous and belong to the two-dimensional Ising universality class. For the transition into the dimer and stripe phases, which occurs for $J_2 < 0$ and $|R| > 0.25$, in contrast, energy-histogram analysis indicates the existence of a tricritical point $R^* \approx 0.4$; for $|R| > R^*$, the transition is continuous, while for $0.25 < |R| < R^*$ it becomes first-order. These results demonstrate how frustration not only shifts the critical temperature but also controls the ground-state degeneracy and the nature of the phase transition, enriching our understanding of competing interactions on two-dimensional lattices.

CRediT authorship contribution statement

Mouhcine Azhari: Writing – review & editing, Writing – original draft, Validation, Software, Methodology, Investigation, Conceptualization. **Hoseung Jang:** Writing – review & editing, Validation, Software, Methodology, Investigation. **Unjong Yu:** Writing – review & editing, Writing – original draft, Validation, Supervision, Software, Methodology, Investigation.

Declaration of competing interest

The authors declare that they have no known competing financial interests or personal relationships that could have appeared to influence the work reported in this paper.

Acknowledgments

This work was supported by GIST Research Project grant funded by the GIST in 2025 and by the National Research Foundation of Korea(NRF) grant funded by the Korea government(MSIT) (No. 2021R1 F1A1052117). M.A. acknowledges financial support by Deutsche Forschungsgemeinschaft, Germany through FOR 2316.

Data availability

Data will be made available on request.

References

[1] Onsager L. Crystal statistics. I. A two-dimensional model with an order-disorder transition. Phys Rev 1944;65(3–4):117. http://dx.doi.org/10.1103/PhysRev.65.117.

[2] Ising E. Beitrag zur theorie des ferromagnetismus. Z. Phys. 1925;31:253–8. http://dx.doi.org/10.1007/BF02980577.

[3] Mihura B, Landau DP. New type of multicritical behavior in a triangular lattice gas model. Phys Rev Lett 1977;38(17):977–80. http://dx.doi.org/10.1103/PhysRevLett.38.977.

[4] Selke W, E. Fisher M. Spatially modulated phase in Ising models with competing interactions. J Magn Magn Mater 1980;15–18:403–4. http://dx.doi.org/10.1016/0304-8853(80)91105-1.

[5] Landau DP. Phase transitions in the Ising square lattice with next-nearest-neighbor interactions. Phys Rev B 1980;21(3):1285–97. http://dx.doi.org/10.1103/PhysRevB.21.1285.

[6] Brandt U, Stolze J. Ground states of the triangular Ising model with two- and three-spin interactions. Z Phys B 1986;64(4):481–90. http://dx.doi.org/10.1007/BF01312843.

[7] Azaria P, Diep HT, Giacomini H. Coexistence of order and disorder and reentrance in an exactly solvable model. Phys Rev Lett 1987;59(15):1629–32. http://dx.doi.org/10.1103/PhysRevLett.59.1629.

[8] Yokota T. Reentrant and successive phase transitions in the Ising model with competing interactions. Phys Rev B 1989;39(1):523–7. http://dx.doi.org/10.1103/PhysRevB.39.523.

[9] Debauche M, Diep HT. Successive reentrances and phase transitions in exactly solved dilute centered square Ising lattices. Phys Rev B 1992;46(13):8214–8. http://dx.doi.org/10.1103/PhysRevB.46.8214.

[10] Grynberg MD, Tanatar B. Square Ising model with second-neighbor interactions and the Ising chain in a transverse field. Phys Rev B 1992;45(6):2876–82. http://dx.doi.org/10.1103/PhysRevB.45.2876.

[11] Morán-López JL, Aguilera-Granja F, Sanchez JM. First-order phase transitions in the Ising square lattice with first- and second-neighbor interactions. Phys Rev B 1993;48(5):3519–22. http://dx.doi.org/10.1103/PhysRevB.48.3519.

[12] Morán-López JL, Aguilera-Granja F, Sanchez JM. Phase transitions in Ising square antiferromagnets with first- and second-neighbour interactions. J Phys: Condens Matter 1994;6(45):9759. http://dx.doi.org/10.1088/0953-8984/6/45/025.

[13] Rastelli E, Regina S, Tassi A. Monte Carlo simulations on a triangular Ising antiferromagnet with nearest and next-nearest interactions. Phys Rev B 2005;71(17):174406. http://dx.doi.org/10.1103/PhysRevB.71.174406.

[14] Malakis A, Fytas NG, Kalozoumis P. First-order transition features of the triangular Ising model with nearest- and next-nearest-neighbor antiferromagnetic interactions. Phys A 2007;383(2):351–71. http://dx.doi.org/10.1016/j.physa.2007.04.051.

[15] Kalz A, Honecker A, Fuchs S, Pruschke T. Phase diagram of the Ising square lattice with competing interactions. Eur Phys J B 2008;65:533–7. http://dx.doi.org/10.1140/epjb/e2008-00359-6.

[16] Lee JH, Song HS, Kim JM, Kim S-Y. Study of a square-lattice Ising superantiferromagnet using the Wang–Landau algorithm and partition function zeros. J Stat Mech Theory Exp 2010;2010(03):P03020. http://dx.doi.org/10.1088/1742-5468/2010/03/P03020.

[17] Jin S, Sen A, Sandvik AW. Ashkin–Teller criticality and pseudo-first-order behavior in a frustrated Ising model on the square lattice. Phys Rev Lett 2012;108(4):045702. http://dx.doi.org/10.1103/PhysRevLett.108.045702.

[18] Ramazanov MK, Murtazaev AK, Magomedov MA. Thermodynamic, critical properties and phase transitions of the Ising model on a square lattice with competing interactions. Solid State Commun 2016;233:35–40. http://dx.doi.org/10.1016/j.ssc.2016.02.012.

[19] Bobák A, Lučivjanský T, Žukovič M, Borovský M, Balcerzak T. Tricritical behaviour of the frustrated Ising antiferromagnet on the honeycomb lattice. Phys Lett A 2016;380(34):2693–7. http://dx.doi.org/10.1016/j.physleta.2016.06.019.

[20] Žukovič M, Borovský M, Bobák A, Balcerzak T, Szałowski K. Spin-glass-like ordering in a frustrated J_1-J_2 Ising antiferromagnet on a honeycomb lattice. Acta Phys Pol A 2021;137:619. http://dx.doi.org/10.12693/APhysPolA.137.619.

[21] Hu Y, Charbonneau P. Numerical transfer matrix study of frustrated next-nearest-neighbor Ising models on square lattices. Phys Rev B 2021;104(14):144429. http://dx.doi.org/10.1103/PhysRevB.104.144429.

[22] Li H, Yang L-P. Tensor network simulation for the frustrated J_1–J_2 Ising model on the square lattice. Phys Rev E 2021;104:024118. http://dx.doi.org/10.1103/PhysRevE.104.024118.

[23] Žukovič M. Critical properties of the frustrated Ising model on a honeycomb lattice: A Monte Carlo study. Phys Lett A 2021;404:127405. http://dx.doi.org/10.1016/j.physleta.2021.127405.

[24] Acevedo S, Arlego M, Lamas CA. Phase diagram study of a two-dimensional frustrated antiferromagnet via unsupervised machine learning. Phys Rev B 2021;103:134422. http://dx.doi.org/10.1103/PhysRevB.103.134422.

[25] Schmidt M, Godoy P. Phase transitions in the Ising antiferromagnet on the frustrated honeycomb lattice. J Magn Magn Mater 2021;537:168151. http://dx.doi.org/10.1016/j.jmmm.2021.168151.

[26] Abalmasov VA, Vugmeister BE. Metastable states in the J_1–J_2 Ising model. Phys Rev E 2023;107:034124. http://dx.doi.org/10.1103/PhysRevE.107.034124.

[27] Yoshiyama K, Hukushima K. Higher-order tensor renormalization group study of the J_1–J_2 Ising model on a square lattice. Phys Rev E 2023;108:054124. http://dx.doi.org/10.1103/PhysRevE.108.054124.

[28] Gangat AA. Weak first-order phase transitions in the frustrated square lattice $J_1 - J_2$ classical Ising model. Phys Rev B 2024;109:104419. http://dx.doi.org/10.1103/PhysRevB.109.104419.

[29] Jang H, Yu U. Monte Carlo study of frustrated Ising model with nearest- and next-nearest-neighbor interactions in generalized triangular lattices. J Stat Mech Theory Exp 2024;2024(7):073204. http://dx.doi.org/10.1088/1742-5468/ad5c58.

[30] Gessert D, Weigel M, Janke W. Partition function zeros of the frustrated $J_1 - J_2$ Ising model on the honeycomb lattice. Entropy 2024;26(11). http://dx.doi.org/10.3390/e26110919.

[31] Diep H, editor. Frustrated spin systems. second ed. Singapore: World Scientific; 2013, http://dx.doi.org/10.1142/8676.

[32] Starykh OA. Unusual ordered phases of highly frustrated magnets: a review. Rep Progr Phys 2015;78(5):052502. http://dx.doi.org/10.1088/0034-4885/78/5/052502.

[33] Lhotel E, Jaubert LDC, Holdsworth PCW. Fragmentation in frustrated magnets: A review. J Low Temp Phys 2020;201(5):710–37. http://dx.doi.org/10.1007/s10909-020-02521-3.

[34] Wales D. Energy landscapes: Applications to clusters, biomolecules and glasses. Cambridge molecular science, Cambridge: Cambridge University Press; 2004, http://dx.doi.org/10.1017/CBO9780511721724.

[35] Vojta M. Frustration and quantum criticality. Rep Progr Phys 2018;81(6):064501. http://dx.doi.org/10.1088/1361-6633/aab6be.

[36] Yahne DR, Pereira D, Jaubert LDC, Sanjeewa LD, Powell M, Kolis JW, et al. Understanding reentrance in frustrated magnets: The case of the $Er_2Sn_2o_7$ pyrochlore. Phys Rev Lett 2021;127(27):277206. http://dx.doi.org/10.1103/PhysRevLett.127.277206.

[37] Shrock R, Tsai S-H. Lower bounds and series for the ground-state entropy of the Potts antiferromagnet on Archimedean lattices and their duals. Phys Rev E 1997;56:4111–24. http://dx.doi.org/10.1103/PhysRevE.56.4111.

[38] Wang L, Sandvik AW. Critical level crossings and gapless spin liquid in the square-lattice spin-1/2 $J_1 - J_2$ Heisenberg antiferromagnet. Phys Rev Lett 2018;121(10):107202. http://dx.doi.org/10.1103/PhysRevLett.121.107202.

[39] Uraga S, Tada Y. Spin nematic order and superconductivity in J_1–J_2 Kondo lattice model on the square lattice. Phys Rev B 2025;111:075110. http://dx.doi.org/10.1103/PhysRevB.111.075110.

[40] Chancellor N, Haas S. Using the J_1–J_2 quantum spin chain as an adiabatic quantum data bus. New J Phys 2012;14(9):095025. http://dx.doi.org/10.1088/1367-2630/14/9/095025.

[41] Zhang X, Zhang W, Liu B. Efficient charging of the quantum battery based on the driven Heisenberg J_1–J_2 model. Adv Quantum Technol 2025;2025:2400683. http://dx.doi.org/10.1002/qute.202400683.

[42] Hovančík D, Kratochvílová M, Haidamak T, Doležal P, Carva K, Bendová A, et al. Robust intralayer antiferromagnetism and tricriticality in the van der Waals compound VBr_3. Phys Rev B 2023;108:104416. http://dx.doi.org/10.1103/PhysRevB.108.104416.

[43] Wildes AR, Lançon D, Chan MK, Weickert F, Harrison N, Simonet V, et al. High field magnetization of $FePS_3$. Phys Rev B 2020;101:024415. http://dx.doi.org/10.1103/PhysRevB.101.024415.

[44] Lee J-U, Lee S, Ryoo JH, Kang S, Kim TY, Kim P, et al. Ising-type magnetic ordering in atomically thin $FePS_3$. Nano Lett 2016;16(12):7433–8. http://dx.doi.org/10.1021/acs.nanolett.6b03052.

[45] Dias PF, Krindges A, Morais CV, Zimmer FM, Mohylna M, Žukovič M, et al. Residual entropy, bicriticality, and tricriticality in the frustrated Ising model on the honeycomb lattice. J Magn Magn Mater 2024;604:172282. http://dx.doi.org/10.1016/j.jmmm.2024.172282.

[46] Dias PF, Schmidt M. Zigzag phase transition in the frustrated Ising honeycomb lattice. Phys Rev B 2023;108:014436. http://dx.doi.org/10.1103/PhysRevB.108.014436.

[47] Richter J, Schulenburg J, Honecker A. Quantum magnetism in two dimensions: From semi-classical Néel order to magnetic disorder. In: Schollwöck U, Richter J, Farnell DJJ, Bishop RF, editors. Quantum magnetism. Lecture notes in physics, vol. 645, Berlin: Springer; 2004, p. 85–153.

[48] Yu U. Ising antiferromagnet on the Archimedean lattices. Phys Rev E 2015;91(6):062121. http://dx.doi.org/10.1103/PhysRevE.91.062121.

[49] Yu U. Ising antiferromagnet on the 2-uniform lattices. Phys Rev E 2016;94(2):022112. http://dx.doi.org/10.1103/PhysRevE.94.022112.

[50] Oitmaa J, Singh RRP. Phase diagram of the $J_1 - J_2 - J_3$ Heisenberg model on the honeycomb lattice: A series expansion study. Phys Rev B 2011;84:094424. http://dx.doi.org/10.1103/PhysRevB.84.094424.

[51] Cabra DC, Lamas CA, Rosales HD. Quantum disordered phase on the frustrated honeycomb lattice. Phys Rev B 2011;83:094506. http://dx.doi.org/10.1103/PhysRevB.83.094506.

[52] Zhang H, Lamas CA. Exotic disordered phases in the quantum J_1-J_2 model on the honeycomb lattice. Phys Rev B 2013;87:024415. http://dx.doi.org/10.1103/PhysRevB.87.024415.

[53] Gao S, McGuire MA, Liu Y, Abernathy DL, Cruz Cd, Frontzek M, et al. Spiral spin liquid on a honeycomb lattice. Phys Rev Lett 2022;128:227201. http://dx.doi.org/10.1103/PhysRevLett.128.227201.

[54] Wang F, Landau DP. Efficient, multiple-range random walk algorithm to calculate the density of states. Phys Rev Lett 2001;86(10):2050–3. http://dx.doi.org/10.1103/PhysRevLett.86.2050.

[55] Betts DD, Lin HQ, Flynn JS. Improved finite-lattice estimates of the properties of two quantum spin models on the infinite square lattice. Can J Phys 1999;77(5):353–69. http://dx.doi.org/10.1139/p99-041.

[56] Maier TA, Jarrell M, Schulthess TC, Kent PRC, White JB. Systematic study of d-wave superconductivity in the 2D repulsive Hubbard model. Phys Rev Lett 2005;95:237001. http://dx.doi.org/10.1103/PhysRevLett.95.237001.

[57] Binder K. Finite size scaling analysis of Ising model block distribution functions. Z Phys B 1981;43(2):119–40. http://dx.doi.org/10.1007/BF01293604.

[58] Metropolis N, Rosenbluth AW, Rosenbluth MN, Teller AH, Teller E. Equation of state calculations by fast computing machines. J Chem Phys 1953;21(6):1087–92. http://dx.doi.org/10.1063/1.1699114.

[59] Janke W. Recent developments in Monte-Carlo simulations of first-order phase transitions. In: Landau DP, Mon KK, Schüttler H-B, editors. Computer simulation studies in condensed-matter physics VII. Berlin: Springer; 1994, p. 29.

[60] Silva CJ, Caparica AA, Plascak JA. Wang–Landau Monte Carlo simulation of the Blume–Capel model. Phys Rev E 2006;73(3):036702. http://dx.doi.org/10.1103/PhysRevE.73.036702.

[61] Azhari M, Yu U. Tricritical point in the mixed-spin Blume–Capel model on three-dimensional lattices: Metropolis and Wang–Landau sampling approaches. Phys Rev E 2020;102(4):042113. http://dx.doi.org/10.1103/PhysRevE.102.042113.

[62] Azhari M, Yu U. Monte Carlo studies of the Blume–Capel model on nonregular two- and three-dimensional lattices: Phase diagrams, tricriticality, and critical exponents. J Stat Mech Theory Exp 2022;2022(3):033204. http://dx.doi.org/10.1088/1742-5468/ac561b.

[63] Jin K, Yu U. Entropy profiles of Schelling's segregation model from the Wang–Landau algorithm. Chaos 2022;32(11):113103. http://dx.doi.org/10.1063/5.0115101.

[64] Azhari M, Yu U. Static universality of the Ising and Blume–Capel models on two-dimensional Penrose tiles. Results Phys 2023;51:106628. http://dx.doi.org/10.1016/j.rinp.2023.106628.

[65] Ramirez AP, Hayashi A, Cava RJ, Siddharthan R, Shastry BS. Zero-point entropy in 'spin ice'. Nature 1999;399(6734):333–5. http://dx.doi.org/10.1038/20619.

[66] Redpath TE, Hopkinson JM. Spin ice on the trillium lattice studied by Monte Carlo calculations. Phys Rev B 2010;82(1):014410. http://dx.doi.org/10.1103/PhysRevB.82.014410.

[67] Žukovič M. Residual entropy of spin-s triangular Ising antiferromagnet. Eur Phys J B 2013;86:283. http://dx.doi.org/10.1140/epjb/e2013-40439-x.

[68] Binder K. Critical properties from Monte Carlo coarse graining and renormalization. Phys Rev Lett 1981;47(9):693–6. http://dx.doi.org/10.1103/PhysRevLett.47.693.

[69] Challa MSS, Landau DP, Binder K. Finite-size effects at temperature-driven first-order transitions. Phys Rev B 1986;34(3):1841–52. http://dx.doi.org/10.1103/PhysRevB.34.1841.

[70] Yu U. Critical temperature of the Ising ferromagnet on the fcc, hcp, and dhcp lattices. Phys A 2015;419:75–9. http://dx.doi.org/10.1016/j.physa.2014.10.001.

[71] Wannier GH. Antiferromagnetism. The triangular Ising net. Phys Rev 1950;79(2):357–64. http://dx.doi.org/10.1103/PhysRev.79.357.

[72] Codello A. Exact curie temperature for the Ising model on Archimedean and Laves lattices. J Phys A 2010;43(38):385002. http://dx.doi.org/10.1088/1751-8113/43/38/385002.

[73] Ashkin J, Teller E. Statistics of two-dimensional lattices with four components. Phys Rev 1943;64:178–84. http://dx.doi.org/10.1103/PhysRev.64.178.

[74] Kadanoff LP, Wegner FJ. Some critical properties of the eight-vertex model. Phys Rev B 1971;4:3989–93. http://dx.doi.org/10.1103/PhysRevB.4.3989.

[75] Cary T, Singh RRP, Scalettar RT. Tricriticality in crossed Ising chains. Phys Rev E 2017;96(4):042108. http://dx.doi.org/10.1103/PhysRevE.96.042108.

[76] Kalz A, Honecker A. Location of the Potts-critical end point in the frustrated Ising model on the square lattice. Phys Rev B 2012;86(13):134410. http://dx.doi.org/10.1103/PhysRevB.86.134410.